Passive Lossless Snubber for PFC AC–DC Converters

Hacı Bodur (iD)**, Hüseyin Yeşilyurt** (iD)**, Erdem Akboy** (iD)

Department of Electrical Engineering, Yıldız Technical University Electric and Electronic Faculty, İstanbul, Turkey

ABSTRACT

In this study, an improved passive lossless snubber cell for the non-isolated pulse-width modulation direct-current (DC)–DC converter family is proposed. The proposed snubber cell provides soft switching for all semiconductor power devices in the converter under wide-input voltage–current and output load ranges. Detailed theoretical analysis is carried out and verified with the implementation of a continuous current mode power-factor correction boost converter having 220-V_AC input, 400-V_DC output, 50-kHz switching frequency, and 1-kW output power. The overall efficiency of the proposed converter at full load increased from 85% in hard-switching conditions to 97.5%, thanks to the proposed lossless passive snubber cell. The application of the proposed snubber cell to other DC–DC converters is also presented.
Keywords: Soft switching, passive snubber cell, pulse-width modulation, DC–DC converter

Introduction

Pulse-width modulated (PWM) direct-current (DC)–DC converters are widely used in industry. Because the switching frequency increases in these converters, the sizes of circuits decrease with the costs. However, in hard-switched converters, the frequency cannot be increased sufficiently because of switching losses and electromagnetic interference (EMI). To increase the switching frequency, soft-switching active or passive snubber cells are used in PWM converters. By means of these snubber cells, switching losses and EMI are reduced, and the total efficiency is increased, thus increasing the frequency and power density [1-19].

Active snubber cells require an additional auxiliary switch and an additional control circuit. Therefore, the converter structure becomes complex and the cost increases. However, in some active snubber cells, the auxiliary switch operates with hard switching and causes considerable power loss and EMI [1]. Additionally, some active snubber cells [1-8] have additional voltage stresses on main and auxiliary power components.

Because passive snubber cells do not have an auxiliary switch, they are easier to implement and are cost-effective. When these snubber cells are used, only the parasitic capacitor energy of the switch cannot be recovered, and the rate at which the switch voltage drops to zero cannot be reduced. However, it is possible to operate all semiconductor elements with soft switching. The occurrence of additional voltage stresses on the switch or main diode and the inability to provide soft switching at light loads are listed in the literature as the main problems of passive snubber cells. Additional voltage stresses on the switch and main diode in passive snubber cells cannot be eliminated, but they can be greatly reduced. Voltage stresses on the auxiliary diodes can be prevented completely. However, [9-12] there are additional voltage stresses on both the switch and the auxiliary diode. According to [13-14], there are only additional voltage stresses on the main diode, but soft switching fails at low input currents. In [15], it was problematic that the main diode turned off with hard switching. Furthermore, reverse recovery energy of the main diode could not be recovered. In the study presented by [16],

Corresponding Author:
Erdem Akboy

E-mail:
eakboy@yildiz.edu.tr

there were additional voltage stresses on the auxiliary diode, and the switch was difficult to turn off.

In this study, a new passive lossless resonant snubber cell is developed for the main non-isolated PWM DC–DC converter families. There are no voltage stresses on the switch and auxiliary diodes, but there are low-value additional stresses on the main diode. The cell can provide soft switching under light-load conditions. To verify the theoretical analysis, the designed snubber cell was applied to the power-factor correction (PFC) boost converter operating in continuous-current mode (CCM). Detailed theoretical analysis was confirmed using an application circuit with an input voltage of 220 VAC, an output voltage of 400 VDC, an output power of 1 kW, and a switching frequency of 50 kHz. The total efficiency of the converter increased from 85% in the hard-switched state to 97.5%, thanks to the designed snubber cell. The PFC boost converter, which operates in CCM, is one of the most difficult converters in terms of the healthy operation of snubber cells, because the input voltage and current continuously vary from zero to peak. Therefore, this converter is preferred for design verification.

Theoretical Method

Definitions and assumptions
The designed circuit diagram of the PFC boost with an improved passive snubber cell is given in Figure 1. This snubber cell combines snubber inductance L_S, snubber capacitor C_S, storage or bulk capacitor C_B, and four auxiliary Diodes: D_{S1}, D_{S2}, D_{S3}, and D_{S4}. The main diode, I_{rr}, is the reverse recovery current. i_{in} is the input current. V_O refers to the output voltage. i_{LS} is the snubber inductance current, and i_{DF} is the boost diode current.

The following assumptions are made to facilitate steady-state analysis during a switching period.

- The input voltage, V_{in}, is constant.
- The output capacitor, C_F, is large enough to accept the output voltage, V_O, as constant.
- The L_F boost inductance is large enough to accept the input current, I_{in}, as constant.
- The L_F boost inductance is considerably larger than the L_S snubber inductance.
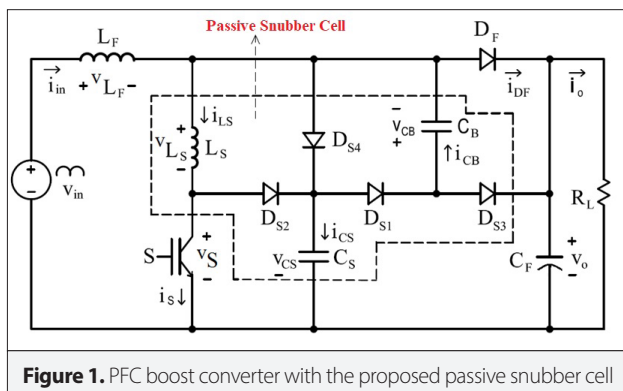
Figure 1. PFC boost converter with the proposed passive snubber cell

- The resonance circuit and semiconductor elements are ideal.
- All diodes except the main diode, D_F, are reversed.

Operation stages
In the designed snubber cell PFC boost converter, nine different intervals occur during one switching period. At high values of the input current, i_{in}, the diode, D_{S4}, is not in the on state. In these conditions, the operation of the snubber cell is equivalent to the snubber cell provided for the DC–DC boost converter in [14]. However, at low input current values, the snubber cell presented by [14] cannot operate, and soft switching cannot be achieved. In the snubber cell presented here, D_{S4} turns on at low input current values, and soft switching is maintained. In the designed converter, when the instantaneous value of the input current is 65% or below, the peak value, D_{S4}, turns on, and the soft switching continues. The input ratio of D_{S4}, according to the input current, is given in Figure 2. The intervals formed during a switching period and the key waveforms of these stages are given in Figures 3a and 3b, respectively.

Initial status
During this interval, the input current is transferred to the load via diode D_F, and the snubber cell is inactive. This range is the same as the turning-off state of the conventional PWM converter, and its duration is determined by the PWM controller. Throughout this range, the following equation exists:

$$i_{DF} = I_{in}. \tag{1}$$

Stage 1 ($t_0 < t < t_2$)
At the beginning of this stage, $i_S = 0$, $i_{LS} = 0$, $i_{DF} = I_{in}$, $v_{CS} = V_O$, and $v_{CB} = 0$. At $t = t_0$, the signal of the switch component is applied, and this stage starts. In this stage, the following equations are valid:

$$i_{LS} = i_S = \frac{V_O}{L_S}(t - t_0), \tag{2}$$

$$i_{DF} = I_{in} - i_{LS} = I_{in} - \frac{V_O}{L_S}(t - t_0). \tag{3}$$

The active switch turns on with zero-current switching (ZCS) because of the snubber inductance, L_S. During this interval, the i_{LS} current of the L_S snubber inductance increases, and the current of diode D_F decreases by i_{DF}. Primarily, at t_1, the i_{LS} current
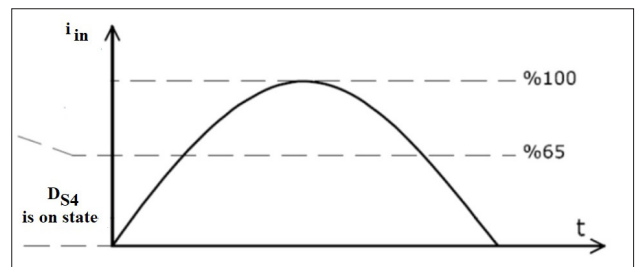
Figure 2. Region of conduction of D_{S4} relative to the input current in the proposed passive snubber cell
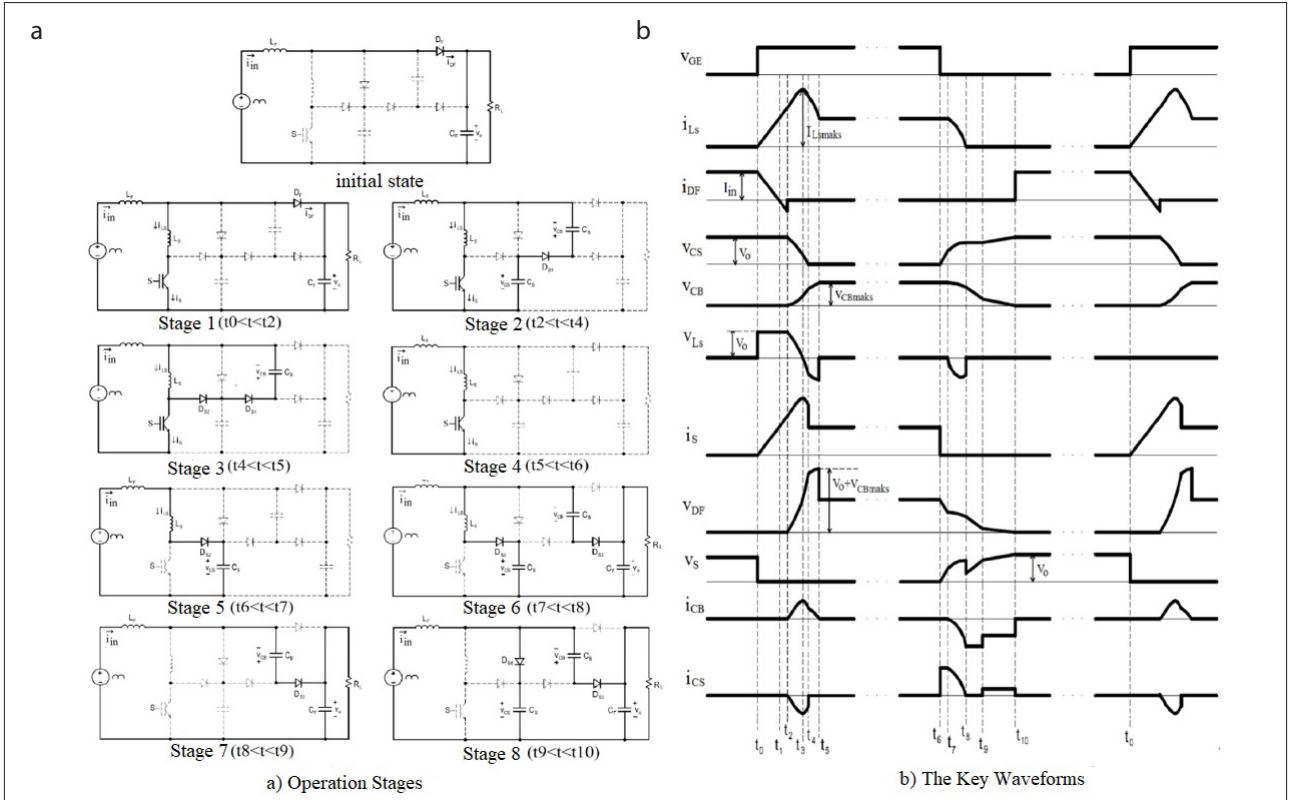
Figure 3. a, b. Equivalent circuit schemes of operation modes (a) and key waveforms in the proposed converter with snubber cell (b)

reaches the value of the input current, i_{in}, and i_{DF} drops to zero. Then, the D_F reverse recovery begins. I_{DF} decreases to $-I_{rr}$ and i_{LS} reaches $I_{in}+I_{rr}$. At t=t_2, the reverse recovery curent falls to zero, the main diode turns off with ZCS because of $L_{s'}$ and also turns off with zero-voltage switching (ZVS) because of C_S and $C_{B'}$ and this interval ends.

Stage 2 ($t_2<t<t_4$)
At the beginning of this stage, $i_s=i_{LS}=I_{in}+I_{rr'}$ $i_{DF}=0$, $v_{CS}=V_{O'}$ and $v_{CB=}0$. After turning off of the $D_{F'}$ D_{S1} turns on, and this stage begins. During this stage, resonance via C_S-D_{S1}-C_B-L_S-S occurs with I_{in}. The snubber inductance current, $i_{LS'}$ reaches its maximum value, $I_{Lsmax'}$ at time t_3. Then, at time $t_{4'}$ the v_{CS} snubber capacitor voltage drops to zero, and the D_{S2} auxiliary diode turns on with ZVS, and this interval ends. The following equations are valid for this interval:

$$i_{LS} = I_{rr} \cos[\omega_1(t - t_2)] + \frac{V_O}{Z_1}\sin[\omega_1(t - t_2)] + I_{in} \tag{4}$$

$$v_{CS} = -\frac{C_e}{C_S}\{-V_O \cos[\omega_1(t - t_2)] + V_O + Z_1 I_{rr} \sin[\omega_1(t - t_2)]\} + V_G \tag{5}$$

$$v_{CB} = \frac{C_e}{C_R}\{-V_O \cos[\omega_1(t - t_2)] + V_O + Z_1 I_{rr} \sin[\omega_1(t - t_2)]\} \tag{6}$$

$$C_e = C_S C_B/(C_S + C_B) \tag{7}$$

$$\omega_1 = 1/\sqrt{L_S C_e} \tag{8}$$

$$Z_1 = \sqrt{L_S/C_e} \tag{9}$$

$$I_{LSmaks} = \sqrt{I_{rr}^2 + (V_O/Z_1)^2} + I_{in} \tag{10}$$

$$t_{23} = \frac{1}{\omega_1}[\pi/2 - arctg\left(\frac{I_{rr}Z_1}{V_O}\right)] = \frac{1}{\omega_1}arctg\left(\frac{V_O}{I_{rr}Z_1}\right) \tag{11}$$

$$t_{24} = \frac{1}{\omega_1}\left(\frac{arcsin\left(\frac{C_S}{C_e} - 1\right).V_O}{\sqrt{V_O^2 + Z_1^2 I_{rr}^2}} + arctg\left(\frac{V_O}{I_{rr}Z_1}\right)\right) \tag{12}$$

$$t_{34} = \frac{1}{\omega_1}\left(\frac{arcsin\left(\frac{C_S}{C_e} - 1\right).V_O}{\sqrt{V_O^2 + Z_1^2 I_{rr}^2}}\right) \tag{13}$$

Stage 3 ($t_4<t<t_5$)
At the beginning of this stage, $i_s=i_{LS}=I_{LS4'}$ $i_{DF}=0$, $v_{CS}=V_{O'}$ and $V_{CB}=V_{CB4}$. The D_{S2} diode turns on, the i_s value drops to $I_{in'}$ and this stage starts. During this interval, the energy in the snubber inductance, $L_{s'}$ is transferred to the storage capacitor, C_B. The following equations apply to this resonance:

$$i_{LS} = (I_{LS4} - I_{in})\cos[\omega_2(t - t_4)] - \frac{V_{CB4}}{Z_2}\sin[\omega_2(t - t_4)] + I_{in} \tag{14}$$

$$v_{CB} = V_{CB4}\cos[\omega_2(t - t_4)] + Z_2(I_{LS4} - I_{in})\sin[\omega_2(t - t_4)] \tag{15}$$

$$Z_2 = \sqrt{L_S/C_B} \tag{16}$$

$$V_{CBmaks} = \sqrt{\frac{L_S I_{rr}^2 + C_S V_O^2}{C_B}} \tag{17}$$

The L_s snubber inductance current, i_{Ls}, decreases to I_{in}, C_B reaches the maximum value of storage capacitor voltage, v_{CB}, V_{CBmax}. D_{S1} and D_{S2} turn off with ZCS because of the snubber inductance, L_s, and this stage ends.

Stage 4 ($t_5<t<t_6$)
This stage starts when diodes D_{S1} and D_{S2} turn off with ZCS. This stage is the same as that of the state of the conventional PWM converter. Its duration is determined by the PWM controller. The following equations apply throughout this stage:

$$i_{in} = I_{LS},$$ (18)

$$v_{CB} = V_{CBmaks},$$ (19)

$$v_{CS} = 0.$$ (20)

Stage 5 ($t_6<t<t_7$)
At this point, $t=t_6$, $i_S=I_{in}$, $i_{DF}=0$, $i_{LS}=I_{in}$, $v_{CS}=0$, and $v_{CB}=V_{CBmax}$ are available. The signal of the switch, S, is removed, it turns off, and D_{S2} turns on under ZVS because of the C_s snubber capacitor. Thus, this interval begins. During this interval, capacitor C_s is charged with a constant input current, I_{in}, and the following equations are applied:

$$v_{CS} = \frac{I_{in}}{C_S}(t - t_6).$$ (21)

The v_{CS} value reaches V_O-V_{CBmax}, D_{S3} is turned on under ZVS and ZCS, and this interval ends. The time obtained by this interval is given below.

$$t_{67} = \frac{C_S}{I_{in}}(V_O - V_{CBmax}).$$ (22)

Stage 6 ($t_7<t<t_8$)
At $t=t_7$, $v_{CS}=V_O-V_{CB}$. The D_{S3} diode turns on under ZVS and ZCS, and this interval begins. Parallel resonance occurs under a constant input current with the path shown in Figure 3a, Stage 6. In this stage, C_s is charged, C_B transfers its energy to the load, and the L_s energy is reset. The following equations apply throughout this stage.

$$i_{Ls} = \left(1 - \frac{C_e}{C_B}\right)I_{in}\cos[\omega_1(t - t_7)] + \frac{C_e}{C_B}I_{in},$$ (23)

$$v_{CS} = V_{CS7} + \frac{C_e}{C_S}Z_1\left(1 - \frac{C_e}{C_B}\right)I_{in}\sin[\omega_1(t - t_7)] + \frac{1}{C_S + C_B}I_{in}(t - t_7),$$ (24)

$$v_{CB} = V_{CBmaks} + \frac{C_e}{C_B}Z_1\left(1 - \frac{C_e}{C_B}\right)I_{in}\sin[\omega_1(t - t_7)] - \frac{1}{C_S + C_B}I_{in}(t - t_7),$$ (25)

$$C_e = C_SC_B/(C_S + C_B).$$ (26)

At the beginning of this stage, the initial current of the snubber capacitor, C_s, is equal to the value I_{in}. Additionally, because the capacitance value of C_s is smaller than the capacitance value of the storage capacitor, C_B, capacitor C_s is charged faster than C_B. In this stage, at low values of the input current, C_s cannot be charged to the output voltage, V_o. If $i_{Ls}=0$, D_{S2} turns off with ZCS, and this stage ends.

Stage 7 ($t_8<t<t_9$)
At $t=t_8$, D_{S2} turns off with ZCS, and this interval starts. During this interval, C_B is discharged with constant input current and

transfers its energy to the load. The following equation is obtained for this stage.

$$v_{CB} = V_{CB8} - \frac{I_{in}}{C_B}(t - t_8).$$ (27)

When the C_B capacitor voltage, V_{CB}, decreases to V_O-V_{CS8}, D_{S4} turns on with ZVS, and this interval ends.

Stage 8 ($t_9<t<t_{10}$)
The D_{S4} diode turns on with ZVS, and this stage begins. At the beginning of this stage, $i_S=0$, $i_{DF}=0$, $i_{LS}=0$, $v_{CS}=V_{CS8}$, and $v_{CB}=VC_{B9}$. Simultaneously, the charge capacitor, C_S, is charged, and charge capacitor C_B is discharged. At $t=t_{10}$, $v_{CS}=V_O$, $v_{CB}=0$, D_{S3} and D_{S4} are turned off under ZVS, D_F is turned on under ZVS, this interval ends, and the initial condition is returned. The following equations are valid throughout this stage.

$$v_{CS} = V_{CS9} + \frac{I_{in}}{C_S + C_B}(t - t_9),$$ (28)

$$v_{CB} = V_{CB9} - \frac{I_{in}}{C_S + C_B}(t - t_9).$$ (29)

Design procedure
The selection criteria of the snubber inductance and capacities of the snubber cell presented in this section will now be given.

Snubber inductance L_s
The L_s snubber inductance is designed to be turned off of the main diode via ZCS and is to be turned on with ZCS of the switch. The snubber inductance for the ZCS process can be selected by considering the following equations [13].

$$\frac{V_o}{L_s}t_r \le I_{inmaks},$$ (30)

$$\frac{V_o}{L_s}3t_{rr} \le I_{inmax}.$$ (31)

Here, t_r is the rise time for the switch, and t_{rr} is the reverse recovery time for the main diode.

For soft switching, L_s must be equal to or greater than the calculated value. A larger L_s can provide less additional current stresses on the switch. However, selecting L_s too large causes transient intervals to take longer, which causes PWM operations to interrupt and increases the current values of the auxiliary diodes.

Snubber capacitor C_s
The C_s snubber capacitor must be selected so that the switch can turn off with ZVS. When the switch is turned off for ZVS operation, C_s selection is made according to the voltage increases from 0 to V_o for a minimum period of time [13]. Thus, the C_s min. value can be selected by considering the following equation.

$$C_S \ge \frac{I_{inmaks}t_f}{V_o}.$$ (32)

Increasing the C_s value makes the switch voltage increase more slowly, making it easier to meet the electromagnetic compatibility standards. However, the very large selection also increases the transient intervals and increases the auxiliary diode cur-

rents. According to Eq. (17), the stress on the main diode causes increases.
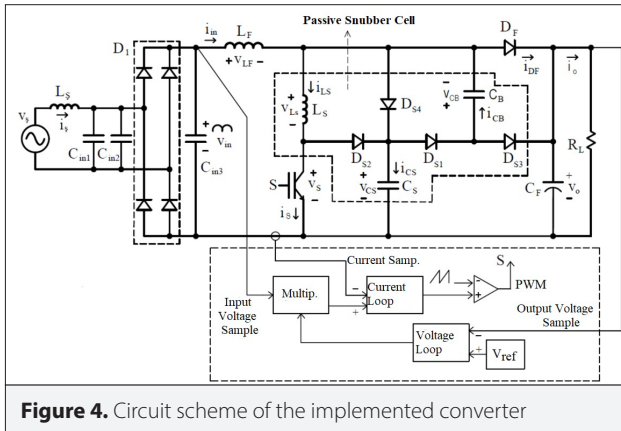
Figure 4. Circuit scheme of the implemented converter

The control mechanism of the proposed converter is given in Figure 4. This control technique is the traditional PFC control technique and it is so easy to implement. Furthermore, the parameters of the implementation circuit according to the design procedure, are given in Table 1.

Experimental Results

Theoretical analysis was confirmed using an application circuit having 220-VAC input, 400-VDC output voltage, 1-kW output power, and 50-kHz switching frequency. The results obtained from the application cycle coincided with the simulation results. In Figure 5, the input voltage, v_{in}, the input current, and the mains current work measurements taken from the application circuit are given. Figure 5(a) shows that the input current followed the rectified input voltage perfectly. The total harmonic distortion of the power factor (99.5% input current of the application circuit) was measured as 1.93%. By means of

Table 1. Parameters of the implementation circuit

Parameter	Symbol	Values	Model
Input Voltage	v_{in}	220 V_{AC}	-
Output Voltage	V_o	400 V_{DC}	-
Output Power	P_o	1 kW	-
Switching Frequency	f	50 kHz	-
Filter Capacitors	C_{in1}, C_{in2}	10 µF, 100 nF	MPP, MKP
DC Capacitor	C_{in3}	680 nF	MKP
Output Capacitor	C_F	1000 µF	DC Capacitor
Boost Inductance	L_F	1 mH	EE70 core
Snubber Inductance	L_s	10 µH	EI30 core -10 turns
Snubber Capacitor	C_s	4,7 nF	MMKP
Bulk Capacitor	C_B	15 nF	MMKP
Auxiliary Diodes	D_{S1}, D_{S2}, D_{S3}, D_{S4}	600 V – 4 A	MUR460-E3/54
Main Diode	D_F	1000V – 12 A	STTH1210D/TO-220AC
Switch	S	600V – 20 A	IKW20N60T/TO247
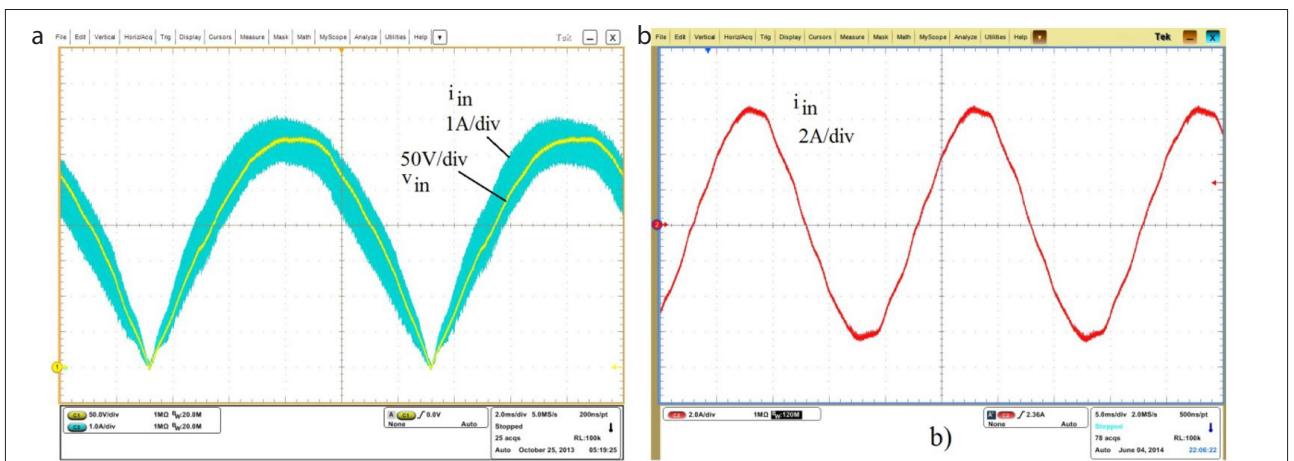
Figure 5. a, b. Input current (i_{in}) (a) and input voltage (v_{in}) grid current (i_{in}) (b)

Figure 6. a, b. Oscillograms of main diode D_F (2 μsn/div) simulation (a) experimental (b)

Figure 7. a, b. Oscillograms of the switch (1 μsn/div) simulation (a), experimental (b)

Figure 8. a, b. Oscillograms of the snubber inductance, L_s, (1 μsn/div) simulation (a) experimental (b)
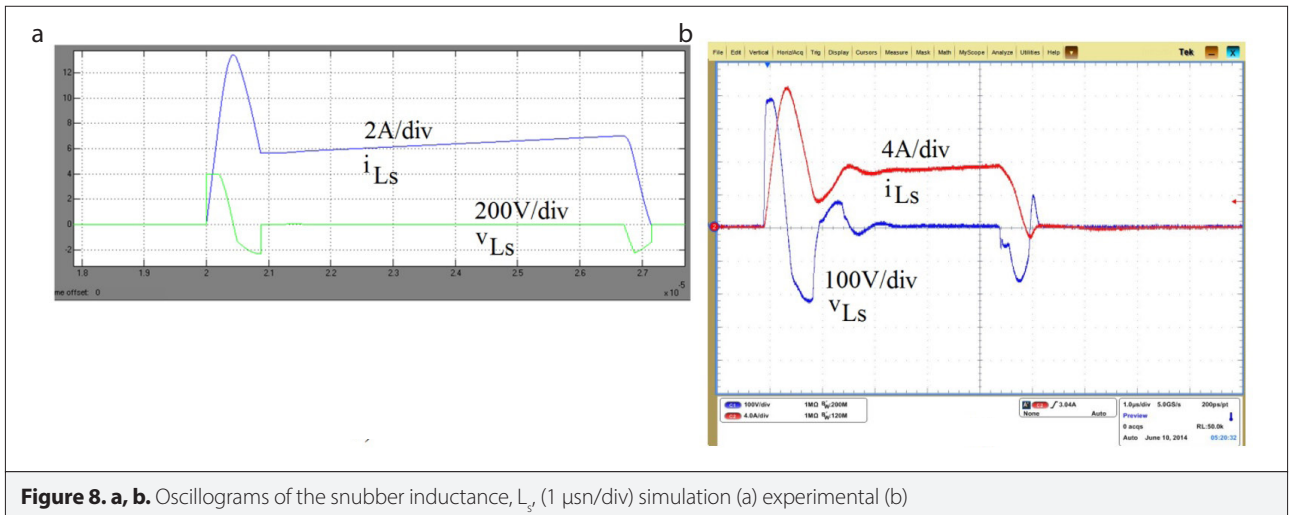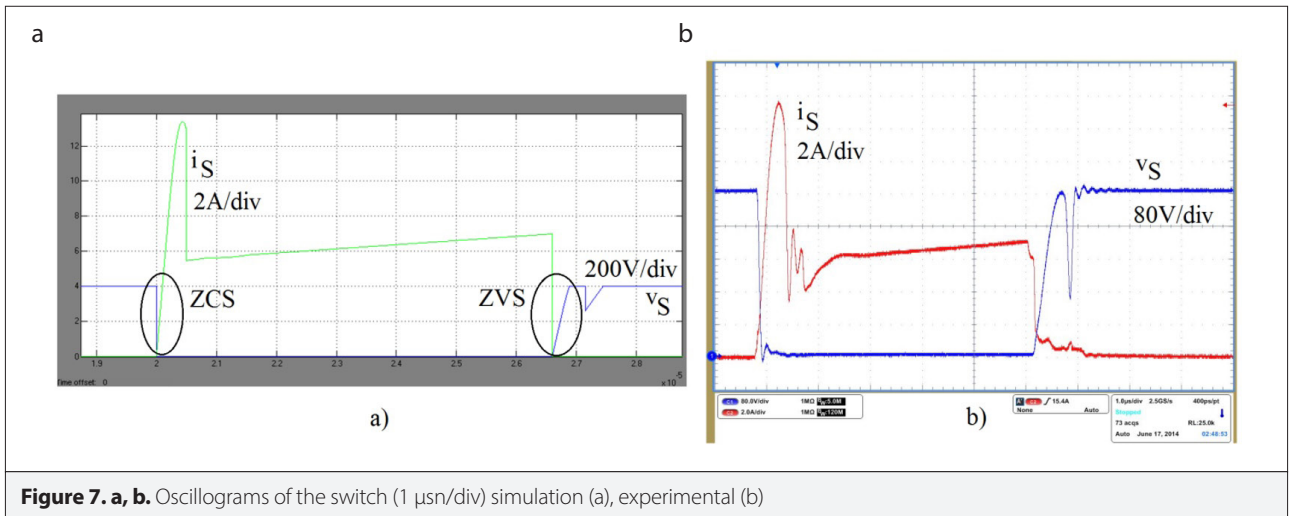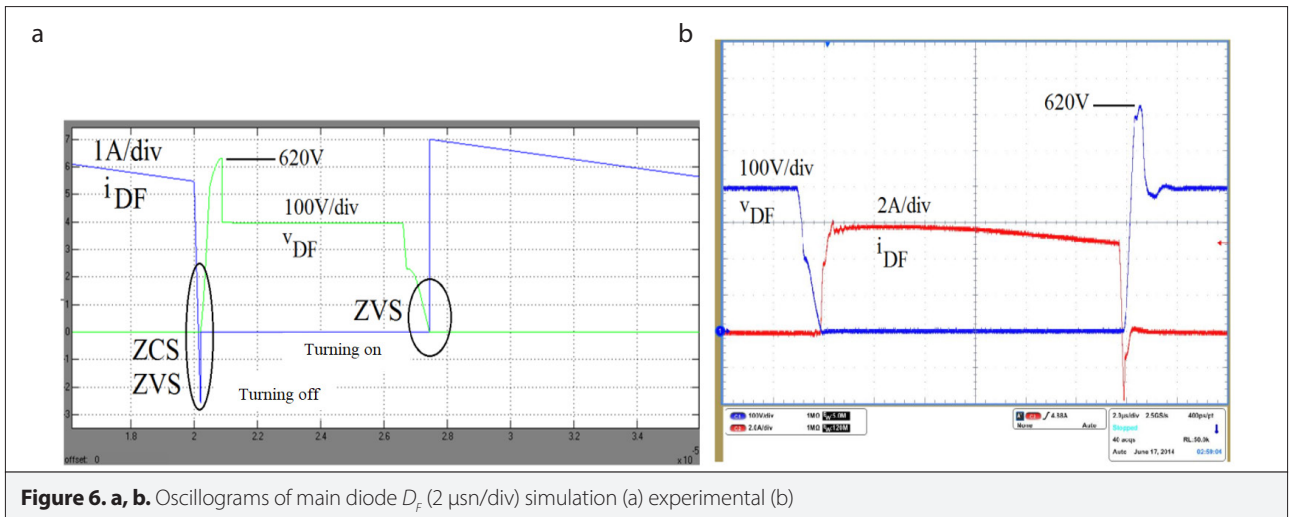
capacitors C_{in1-3}, high frequency components of the input current were filtered to draw the filtered current from the line. The main current is given in Figure 5(b).

In Figure 6, measurements of the main diode, D_F, are given at a 2-μs/div time scale. Figure 6(a) shows the simulation, and Figure 6(b) shows the results from the application circuit. Figure 6

a

b
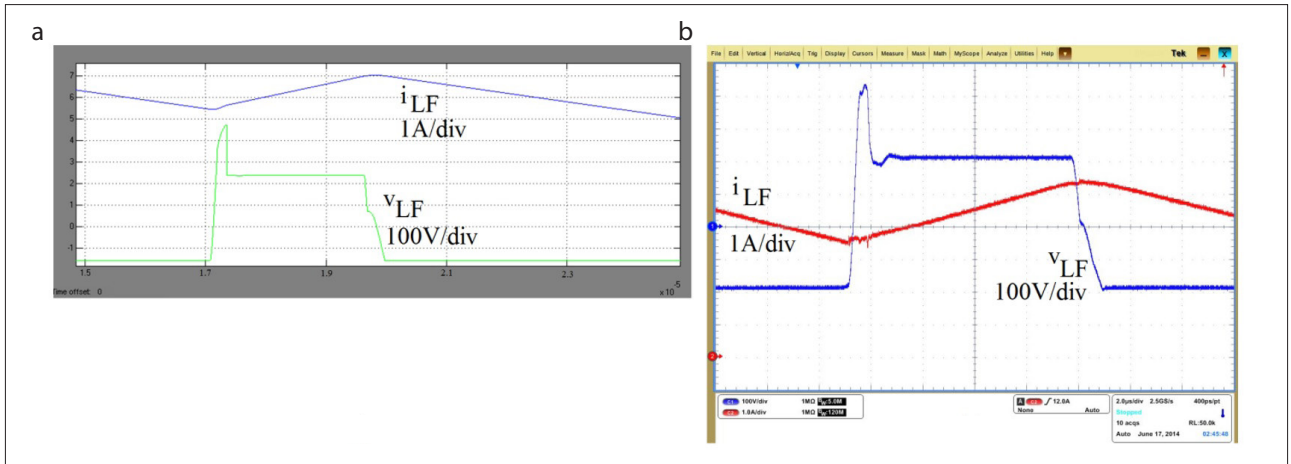
Figure 9. a, b. Oscillograms of the boost inductance, L_F, (1 μsn/div) simulation (a) experimental (b)
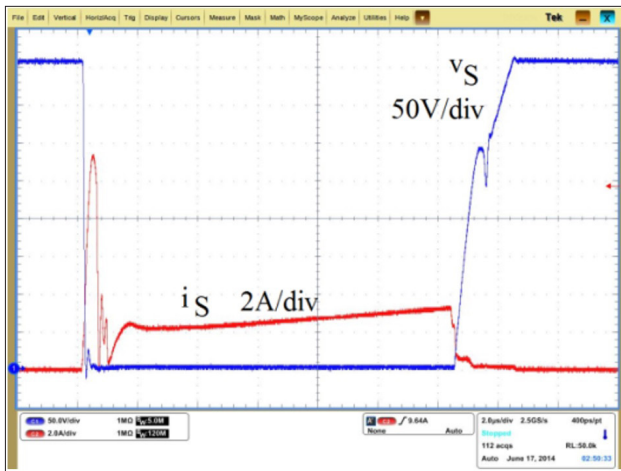
Figure 10. Experimental waveforms of the switch current and voltage under low input voltages (1 μsn/div)
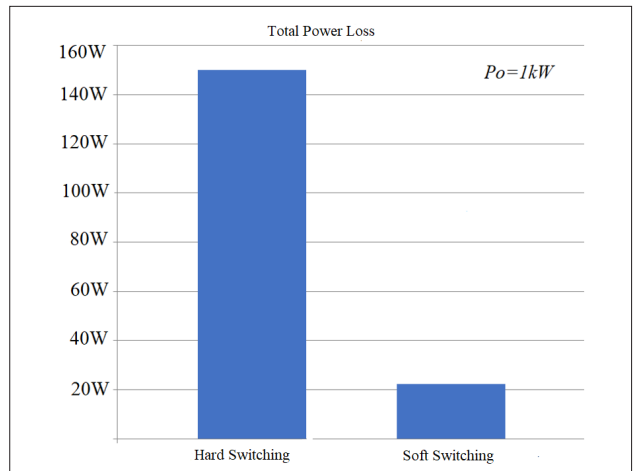
Figure 12. Total power losses in hard- and soft-switching converters, comparatively
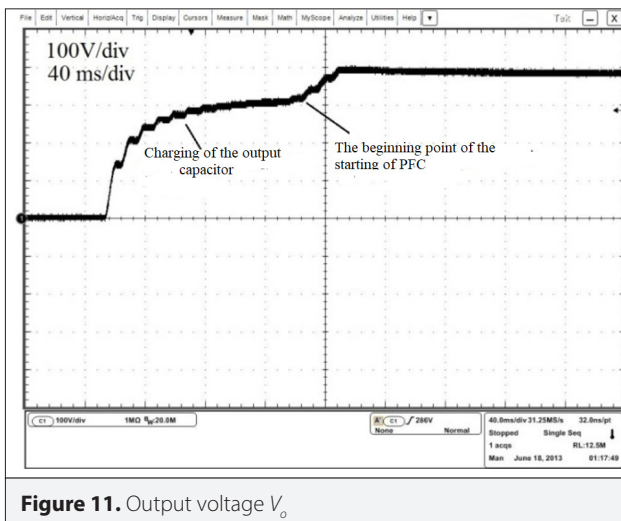
Figure 11. Output voltage V_o

shows that the main diode, D_F, operated under soft switching, turns off with ZCS and ZVS, and turned on with ZVS.

In Figure 7, measurements of key element S are given at a 1mikroseconds/div scale. Figure 7(a) shows the simulation, and Figure 7(b) shows the results from the application circuit. Figure 7 shows that the switch operated under soft switching and is turned on by ZCS and is turned off by ZVS. In Figure 8, the measurements of snubber inductance, L_s, are given at a 1-μs/div scale. In Figure 9, the measurements of the boost inductance, L_F, are given at a 1-μs/div scale. It can be seen that the fluctuation amount of the input current was about 1.5 A. In Figure 10, measurements of the key element, S, for the low current value, are given at a 2-μs/div scale. Here, it is seen that the soft switching was also maintained for the low current value. The output voltage, V_o, is given in Figure 11. After the converter was charged with a charging circuit, the PFC controller allowed the output to begin with a soft start. Figure 12 shows comparative power losses for 1-kW output power of hard- and soft-switching converters. Soft switching reduces power total power loss by 85%, from 150 to 22.5 W. The picture of the application circuit is given in Figure 13.

Figure 13. Photograph of implementation of the proposed soft-switching PFC boost converter
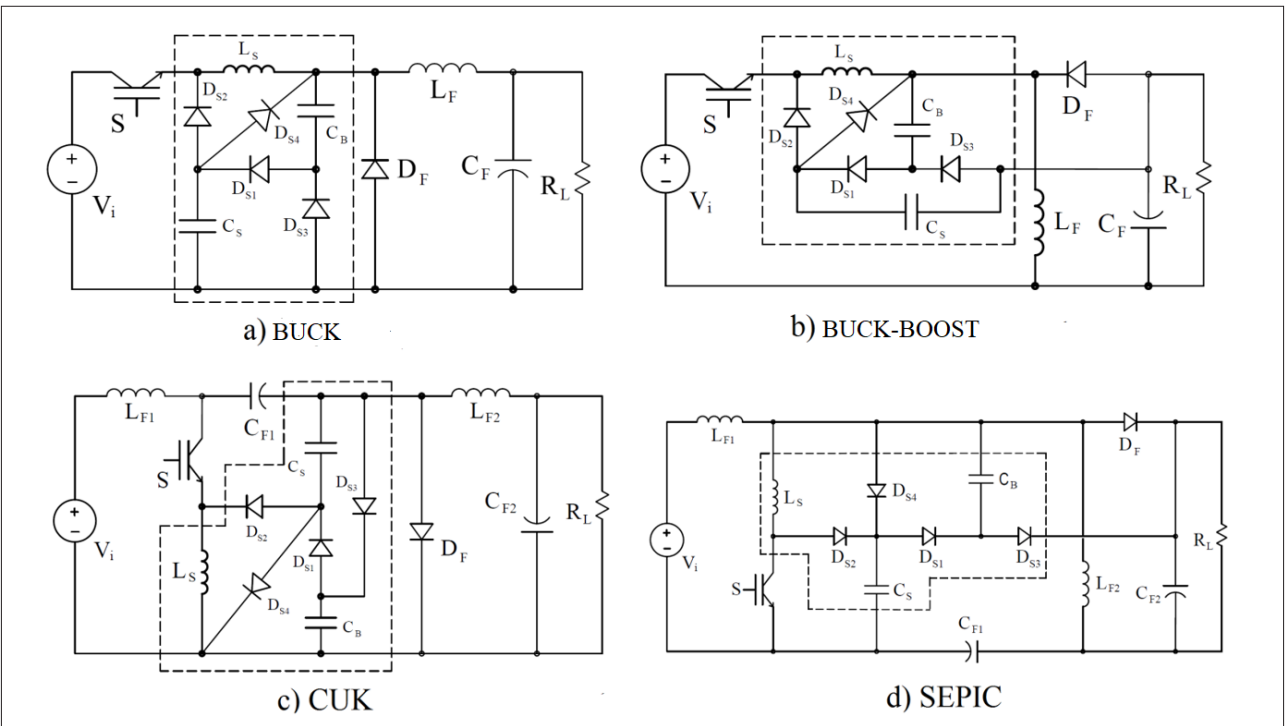
Figure 14. Applying the proposed snubber cell to other basic non-isolated DC–DC converters

All advantages of the snubber cell, including the maintenance of soft switching at low input currents, apply to other non-isolated PWM DC–DC topologies. The circuit diagrams of the buck, buck-boost, CUK-, and SEPIC-type DC–DC converters to which the presented snubber cell was applied are given in Figure 14. There, the snubber cells are enclosed by the dotted line. All auxiliary diodes were subjected to V_{CB} and maximum load current.

Conclusion

In this study, we presented an improved lossless passive snubber cell for non-isolated PWM DC–DC converter families.

Theoretical analysis is confirmed by the application of a PFC boost converter with CCM for 220-VAC input, 400-VDC output, 50-kHz switching frequency, and 1-kW output power. Owing to the provided snubber cell, all semiconductor components were operated with soft switching over a wide range of input voltages and currents. The total efficiency of the applied PFC boost converter in the hard-switched state increased from 85 to 97.5%, thanks to the lossless snubber cell provided. Because non-isolated PWM DC–DC converters are widely used in the industry, the lossless passive snubber cell should play an important role in energy efficiency.

References

1. C. J. Tseng, C. L. Chen, "Novel ZVT PWM converters with active snubbers", IEEE Trans Power Electron, vol. 13, no. 5, pp. 861-9, 1998. [CrossRef]
2. C.M.O. Stein, H.L. Hey, "A true ZCZVT commutation cell for PWM converters", IEEE Trans Power Electron, vol. 15, no. 1, pp. 185-93, 2000. [CrossRef]
3. G. Hua, E. X. Yang, Y. Jiang, F. C. Lee, "Novel zero-current-transition PWM converters", IEEE Trans Power Electron, vol. 9, no. 6, pp. 601-6, 1994. [CrossRef]
4. H. Bodur, S. Yıldırmaz, "A new ZVT snubber cell for PWM-PFC boost converter", IEEE Trans Ind Electron, vol. 64, no. 1, pp. 300-9, 2017. [CrossRef]
5. D. Y. Lee, M. K. Lee, D. S. Hyun, I. Choy, "New zero-current-transition PWM DC/DC converters without current stress", IEEE Trans Power Electron, vol. 18, no. 1, pp. 95-104, 2003. [CrossRef]
6. H. Bodur, A.F. Bakan, "A new ZVT-ZCT -PWM converter", IEEE Trans Power Electron, vol. 19, no. 3, pp. 676-84, 2004. [CrossRef]
7. H. Bodur, İ. Aksoy, A. F. Bakan, "A new ZVT-ZCT -PWM converter", IEEE Trans Power Electron, vol. 25, no. 8, pp. 2093-105, 2010. [CrossRef]
8. N.S. Tıng, Y. Şahin, İ. Aksoy, "Analysis, design and implementation of a zero-voltage-transition interleaved boost converter", J Power Electron, vol. 17, no. 1, 41-55, 2017. [CrossRef]
9. M. R. Amini, H. Farzenahfard, "Novel family of PWM soft-single-switched DC-DC converters with coupled inductors", IEEE Trans Ind Electron, vol. 56, no. 6, pp. 2108-14, 2009. [CrossRef]
10. T. Zhan, Y. Zhang, J. Nie, Y. Zhang, Z. Zhao, "A novel soft-switching boost converter with magnetically coupled resonant snubber", IEEE Trans Power Electron, vol. 29, no. 11, pp. 5680-7, 2014. [CrossRef]
11. Y. Şahin, N. S. Ting, "Soft switching passive snubber cell for family of PWM DC-DC converters", Electrical Enginnering, vol. 100, pp. 1785-96, 2018. [CrossRef]
12. M. Mohammadi, E. Adib, M. R. Yazdani, "Family of soft-switching single-switch PWM converters with lossless passive snubber", IEEE Trans Ind Electron, vol. 62, no. 6, pp. 3473-81, 2015.
13. H. Bodur, A. F. Bakan, M. Baysal, "A detailed analytical analysis of a passive resonant snubber perfectly constructed for pulse width modulated d.c-d.c buck converter", Electrical Enginnering, vol. 85, pp. 45-52, 2003. [CrossRef]
14. C. J. Tseng, C. L. Chen, "A passive lossless snubber cell for non-isolated PWM DC/DC converters", IEEE Trans Ind Electron, vol. 45, no. 4, pp. 593-601, 1998. [CrossRef]
15. R. T. H. Li, H. S. H. Chung, A. K. T. Sung, "Passive lossless snubber for boost PFC with minimum voltage and current stress", IEEE Trans Power Electron, vol. 25, no. 3, pp. 602-13, 2010. [CrossRef]
16. J. J. Yun, H. J. Choe, Y. H. Hwang, Y. K. Park, B. Kang, "Improvement power-conversion efficiency of a DC-DC boost converter using a passive snubber circuit", IEEE Trans Ind Electron, vol. 59, no. 4, 1808-14, 2012. [CrossRef]
17. H. Bodur, A. F. Bakan, "A new ZVT PWM DC-DC converter", IEEE Trans Power Electron, vol. 17, no. 1, pp. 40-7, 2002. [CrossRef]
18. R. Balamurugan, V. Kamsala, R. Nithya, "Current fed full bridge converter with voltage double for photovoltaic system applications", IU-JEEE, vol. 14, no. 2, pp. 1779-84, 2014.
19. W. Yuan, A. Tang, X. Zhang, S. Wang, "Voltage and power loss control in distribution system using UPFC", IU-JEEE, vol. 11, no. 2, pp. 1413-7, 2011.

Haci Bodur (M'00) was born in Ordu, Turkey, in 1959. He received the B.S., M.S., and Ph.D. degrees in electrical engineering from Yildiz Technical University, Yildiz, Turkey, in 1981, 1983, and 1990, respectively. He was employed as a Research Assistant from 1982 to 1986, a Lecturer from 1986 to 1991, an Assistant Professor from 1991 to 1995, and an Associate Professor from 1995 to 2002, in the Department of Electrical Engineering, Yildiz Technical University, Turkey, where, since 2002, he has been a Professor. He has published over 50 journal and conference papers in the area of power electronics. He also took part in more than 10 research projects concerning power electronics. His research has been concentrated on the areas of motor drives, power factor correction, uninterruptable and switching power supplies, high frequency power conversion, and active and passive snubber cells in power electronics

Huseyin Yesilyurt, was born in Adana, Turkey, in 1988. He received the B.S. degree in electrical and electronics engineering from Sakarya University, Turkey, in 2010. He received M.S. degree and PHd in electrical engineering from Yıldız Technical University (YTU), Turkey, in 2013 and 2019. He was research assistant in department of electrical and electronics engineering at Abant Izzet Baysal University (AIBU), in 2011-2012. He was assistant specialist working on welding machines at Eczacıbaşı-Lincoln Electric-Askaynak in 2012-2015. He was welding machines R&D engineer at Gedik Welding in 2015-2017. He was R&D specialist at Arcelik in 2017-2019. He has been R&D engineer in TUBITAK, since 2019.He has worked on various research projects concerning power electronics. His current research interests include DC-DC converters, inverters, power factor correction (PFC), soft switching, active and passive snubber cells and welding machines.

Erdem Akboy was born in Istanbul, Turkey, in 1987. He received B.S. degree in electrical-electronics engineering from Sakarya University, Sakarya, Turkey, in 2009, M.S., and Ph.D. degrees in electrical engineering from Yildiz Technical University, Esenler, Turkey, in 2012 and 2018, respectively, where he is currently a research assistant. His current research interests include soft switching, grid connected converter, power factor correction (PFC), inverters, and DC-DC converters.